NUMERICAL SIMULATION OF DEFLAGRATION-TO-DETONATION TRANSITION BY COUPLED FLAME TRACKING – PARTICLE METHOD

Frolov S. M., Ivanov V. S., Smetanyuk V. A.
Semenov Institute of Chemical Physics, Russian Academy of Sciences

ABSTRACT

The objective of the study outlined in this paper was to develop the computationally efficient algorithm for multidimensional numerical simulation of deflagration-to-detonation transition (DDT) in gas-fueled air-breathing pulse detonation engine (PDE). It is implied, that the availability of such an algorithm will allow for more realistic estimates of PDE performances (specific impulse, thrust, etc.) than those obtained with the presumption of direct detonation initiation. The new algorithm is based on the coupled Flame Tracking – Particle (FTP) method implemented into the standard CFD code solving the Reynolds Averaged Navier–Stokes equations by the control-volume technique. The coupled methodology has been applied to the 2D numerical simulation of DDT in a straight smooth-walled PDE channel 3 m long filled with the stoichiometric propane – air mixture at normal initial conditions. The fuel-based specific impulse was estimated as 2280 s which is close to the value obtained for the conditions of direct detonation initiation.

KEYWORDS: Deflagration-to-Detonation Transition; Numerical Simulation; Pulse Detonation Engine; Propulsion Performance

INTRODUCTION

Realistic estimates of PDE performances (specific impulse, thrust, etc.) require consideration of DDT rather than direct detonation initiation in the PDE tube. Despite the DDT phenomenology is currently well understood [1] its adequate numerical simulation is still not possible. The reason is the necessity of resolving a wide spectrum of length and time scales inherent in the DDT phenomenon and therefore the need in extremely high CPU power.

The classic mechanism of DDT in a straight smooth tube includes several stages [2, 3], namely, (1) forced mixture ignition with the formation of a laminar flame, (2) progressing increase in the rate of combustion because of the appearance of instabilities and subsequently turbulent flow ahead of the flame front, (3) shock wave formation and strengthening ahead of the accelerating flame front, and (4) self-ignition of the shock-compressed mixture in the region between the shock wave and flame front [4] ("explosion in the explosion" [5]) resulting in the formation of an overdriven detonation wave and then (5) self-sustaining Chapman–Jouguet (CJ) detonation. The time and distance of the DDT are known to be largely determined by the first three stages [6]. Detonation in air mixtures of hydrocarbon fuels requires that the "visible" velocity of the turbulent flame front in the laboratory coordinate system be higher than 1000 m/s [7]. At such a flame front velocity, the shock wave running ahead has a velocity higher than 1300 m/s (the shock wave Mach number is $M \approx 3.8$), and the pressure and temperature of the explosive mixture behind it are higher than 1.7 MPa and 1200 K, respectively.

The mechanism of DDT in tubes with regular obstacles [3, 8] is in many respects similar to the mechanism [2–6] described above. There are also important differences. First, the flame is accelerated much more quickly in a tube with obstacles because of the additional turbulization of a fresh explosive mixture when it flows around obstacles. Second, there appear new possibilities for gas ignition. A gas can be autoignited in the shock wave reflected from an obstacle or (if obstacles are large) because of mixing of directed jets of hot combustion products with a cold fresh explosive mixture.

At present, there exist few attempts of numerical simulation of DDT in gases. The most successful is seemingly one by Oran and Gamezo who published a series of papers on DDT in hydrogen–air mixtures in channels with regular obstacles [9, 10]. They solved both 3D and 2D Navier–Stokes equations coupled with the energy conservation equation and the kinetic equation for the single-stage overall chemical reaction. Despite the results of [9, 10] revealed some salient features of flame acceleration in the obstructed channels, the model applied in [9, 10] cannot be used for quantitative predictions. This model does not make a difference between the chemical kinetics of combustion in the flame front and chemical kinetics of autoignition. As is

known, the reactions in flame do not exhibit ignition delays as the reactive mixture is ignited due to heat and active species diffusion from the high-temperature reaction zone. At autoignition, neither heat nor active species are supplied from outside and therefore the initial increase of the reaction rate is significantly slower than in the flame and the main role is played by relatively slow chain origination reactions. The latter means that the reaction rate constant in the overall reaction mechanism describing preflame autoignition should be significantly lower than that describing the reaction in the flame front. As a result, the use of identical reaction rate constants for both preflame and flame reactions in [9, 10] can become a reason of significant overestimation of preflame reaction rates.

The objective of any combustion model is to provide correct values of mean reaction rates regardless the combustion mode in a turbulent reactive flow. The mean reaction rate can be obtained provided one knows the reaction kinetics and the local instantaneous fields of temperature and species concentrations. The development of reaction kinetics is the separate task which is independent of combustion modeling. The only relevant issue is the CPU time required for calculating instantaneous reaction rates. This issue can be overcome by applying properly validated short overall reaction mechanisms and/or look-up tables. The local instantaneous fields of temperature and species concentrations are usually not known. Therefore one has to replace this lacking information by a combustion model.

There exist many combustion models both for laminar and turbulent flows. If chemistry is fast as compared to mixing, the Eddy-Break-Up model can be used [11]. It is simple but has a limited range of validity. There is a whole class of statistical combustion models (based on the formalism of probability density functions) with probabilistic representation of turbulence and its interaction with chemistry [12]. Despite many attractive features, this approach is still not capable of operating with complex chemistry due to inadequate CPU requirements. Moreover, such approaches do not resolve different scales in the turbulent flow and their energy content. Instead, all scales are treated indifferently whereas their effect on combustion and flame is different. Nevertheless, these approaches look very promising for treating autoignition problems. The other class of models deals with a flamelet approach [13]. In this approach, the instantaneous flame is assumed to consist of localized reactive sheets, which are transported by the flow and wrinkled by turbulent eddies. The flamelet approach is applicable when the characteristic turbulent scales are larger than a typical flame thickness. This condition is satisfied in many practical situations. The flamelet models are usually based on the flame surface density concept or apply probability density functions. One of the most attractive flamelet models is based on the balance equation for the flame surface density. This equation governs the transport of the mean reactive surface by the turbulent flow and includes physical mechanisms responsible for flame surface area production and destruction.

The approach used within this study is also based on considering the flame surface area. However, to speed-up calculations, instead of solving the partial differential equation for the flame surface density, it implies tracing of the mean reactive surface and application of the laminar/turbulent flame velocity concepts.

FLAME TRACKING METHOD

The approach outlined below will be referred to as the subgrid model of laminar/turbulent combustion. Let us first explain the essence of the model on the example of laminar flame propagation. The flame surface shape and area can be found based on the Huygens principle (Fig. 1): Each elementary portion of the flame surface *a-b-c-…-i-j-k* displaces in time due to burning of the fresh mixture at local velocity u_n (normal to the flame surface) and due to convective motion of the mixture at local velocity V (see segment *g-h*). The local instantaneous velocity u_n can be taken from the look-up tables including in general the effects of mixture dilution with combustion products, flame stretching, and flammability limits. The local instantaneous velocity V can be calculated using a high-order interpolation technique (e. g., using the velocity values in nodes 1 to 9 in Fig. 1). In Fig. 1, the flame surface is represented by straight line segments. In 3D calculations, the flame surface will be represented by connected triangles.

The energy release rate in the computational cell, Q, is composed of two terms: energy release due to frontal combustion, Q_f, and energy release due to volumetric reactions, Q_f. The first term Q_f can be

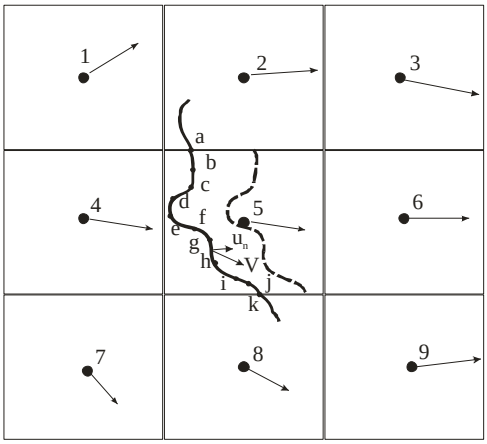

Figure 1: Laminar flame subgrid model.

calculated based on the estimated instantaneous flame surface area S_n and the laminar flame propagation velocity u_n:

$$\dot{Q}_f = \sum S_{ni} u_{ni} \tag{1}$$

where summation is made over all flame segments (e.g., segment *g-h* in Fig. 1) in the cell. The second term Q_v can be calculated using a particle method (see below).

In the turbulent flow field, a pulsating velocity vector distorts the "mean" reactive (flame) surface as shown schematically in Fig. 2 by the thin wrinkled solid curve. The local instantaneous flame wrinkling can be taken into account by proper increasing the normal flame velocity, or in other words, by introducing a concept of local turbulent flame velocity u_T. The local turbulent flame velocity (e.g., at segment *g-h* in Fig. 2) is defined as

$$u_T = u_n S / S_n \tag{2}$$

where S is the surface area of the wrinkled flame at a given segment and S_n is the surface area of the equivalent "planar" flame (straight line *g-h* in Fig. 2).

The problem now is to find the way of calculating u_T. In the theory of turbulent combustion, there are many correlations between u_T and u_n. One of the classical correlations is Shchelkin formula [14]:

$$u_T \approx u_n \sqrt{1 + u'^2 / u_n^2} \tag{3}$$

where u' is the local turbulence intensity, related to the turbulent kinetic energy or to pulsating velocity correlations. Instead of Eq. (3) one can use other available correlations for the turbulent flame velocity.

One can apply the Huygens principle to model only the "mean" shape of the turbulent flame (solid curve *a-b-c-d…-i-j-k* in Fig. 2): each elementary portion of the flame surface *a-b-c-…-i-j-k* displaces in time due to burning of the fresh mixture at local velocity u_T (normal to the flame surface) and due to convective motion of the mixture at local velocity V (see segment *g-h*). The new "mean" flame position is shown by the thick dashed curve in Fig. 2.

The mean energy release rate in the cell, Q, is composed of two terms: energy release due to frontal combustion, Q_f, and energy release due to volumetric combustion, Q_v. The first term Q_f can be calculated based on the estimated "mean" flame surface area and the turbulent flame propagation velocity using Eq. (3) (or other correlations). Equation (3) relates the turbulent flame velocity to laminar flame velocity (tabulated) and local turbulence intensity (provided by any model of turbulence). Based on such an equation one can calculate the mean (frontal) energy release rate in the computational cell as the sum

$$\dot{Q}_f = \sum S_{ni} u_{Ti} \tag{4}$$

where index *i* relates to the flame surface segment (e.g. *g-h* in Fig. 2). The second term Q_v can be calculated using a particle method (see below).

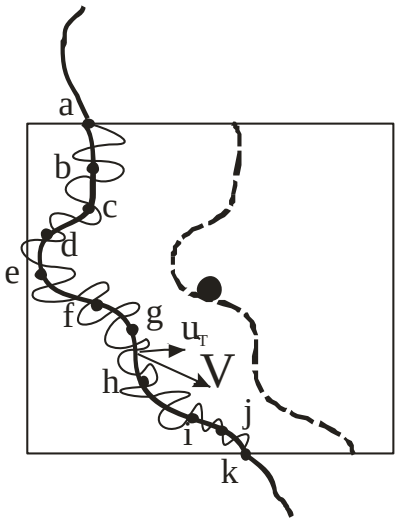

Figure 2: Turbulent flame subgrid model.

Thus, the subgrid model of turbulent premixed combustion does not differ much from that of the laminar premixed combustion, except for using u_T instead of u_n. Moreover, the formulae like Eq. (3) are asymptotically valid for the subgrid model of laminar combustion (when $u' \to 0$, $u_T \to u_n$). It stands to reason that the turbulent combustion model will be also valid for the laminar combustion as a limiting case. This is one of model advantages. This feature will allow using the same model to calculate the initial laminar flame kernel growth from the spark ignition with continuous transition to turbulent combustion. The subgrid combustion model under consideration does not contain tuning parameters (some parameters can be introduced with the equations replacing Eq. (3)). This is the other important model advantage. The additional advantage of the model is that, when coupled with the particle method, it will cover both possible modes of premixed combustion, namely, frontal and volumetric.

It is expected that the accuracy of the computational results will be mainly affected by the turbulence model used. The main problem in implementing such a combustion model into a CFD code is the development of an efficient algorithm for "mean" flame-shape tracing inside computational cells. This algorithm should meet the constraints on the flame-front continuity, connectivity, etc., and the constraints on the CPU time consumption.

PARTICLE METHOD

The particle method allows continuous monitoring of preflame and postflame reactions using the kinetic database [15]. The preflame zone exhibits volumetric reactions of fuel oxidation, formation of intermediate products like alcohols, aldehydes, peroxides, etc. In general, the preflame reactions are inhomogeneous due to inhomogeneous distributions of temperature and main species concentrations. The preflame reactions can result in the localized energy release. For example, low-temperature cool-flame oxidation of n-alkane fuels can result in the release of up to 10%–15% of the total reaction heat. Thus, in general, two-way coupling approach has to be applied for the preflame reactions, however in some cases one-way coupling is also possible. The direct (and CPU time consuming) way to calculate the volumetric reaction rates is to solve the equations of chemical kinetics in the preflame zone in each computational cell. To shorten the CPU time, one can introduce a certain number of trace Lagrangian particles which will move in the preflame zone according to the local velocity vector. In each particle, the preflame reactions will proceed at the rates determined by its instantaneous temperature and species concentrations. For determining the time and location of preflame autoignition there will be a need in adopting a certain criterion. Such a criterion can be based on the fixed rate of temperature rise in the particle, e.g., 10^6 K/s.

In case of two-way coupling, the ignition delay is calculated in each particle based on its temperature and species concentrations and the mean (over all particles in cell) reaction rate directly affects the mean flow pattern. When an autoignition criterion is met in one or several particles, new (forced) ignition sites in the preflame zone can be automatically introduced. In general, these ignition sites give birth to new

laminar/turbulent flame kernels or, if the preflame reactions are fast, they result in the induction (spontaneous) flames and volumetric combustion. The number of particles in the preflame zone can be much less than the number of computational cells. For keeping the number of particles at a reasonable level, the consistent procedures of particle cloning and clustering should be developed. The preflame particles are traced until the entire geometry is traversed by the frontal or volumetric combustion.

KINETIC DATABASE

The coupled FTP algorithm is supplemented with the database of tabulated laminar flame velocities for the stoichiometric propane – air mixture in the wide range of initial temperature (from 300 to 1000 K), pressure (from 0.1 to 10 MPa), and combustion product concentrations (up to nearly 100%) as well as the reaction kinetics of fuel autoignition [15]. The look-up tables contain information on flammability limits to identify the conditions of flame quenching.

RESULTS OF CALCULATIONS

The coupled FTP method has been developed and implemented into the standard CFD code (here, AVL FIRE). The results of integrated code validation for flame propagation in enclosures including the effects of two-stage preflame autoignition are presented elsewhere [16]. As an example of code performance for accelerating flames in long channels with one open end, let us consider the results of four 2D test cases with flame acceleration in the straight rectangular 40x40 mm smooth-walled channels of 2.6, 3.5, 5.1, and 6.1 m long filled with the stoichiometric propane – air mixture at normal initial conditions as used in experiments [17]. In the experiments, the mixture was initially quiescent and ignition took place at approximately 1 cm from the closed end of the channels.

Figure 3 compares the results of calculations with the experiments in terms of the time histories of the distance traveled by the flame. Solid curves correspond to the predicted results whereas the dashed curves correspond to the measurements. The walls of the channel were assumed isothermal ($T_w = 293$ K). At the open end, a constant-pressure ($p_0 = 0.1$ MPa) boundary condition was applied. The use of nonreflecting boundary conditions [18] at the walls of a buffer volume of a larger cross section attached to the open end of the channels did not affect significantly the results of calculations leading however to increasing CPU time. The stoichiometric propane – air mixture was assumed initially quiescent at $T_0 = 293$ K and $p_0 = 0.1$ MPa. The initial flame kernel was taken as a circle 1 mm in radius with the center located at 1 cm from the closed end-wall at the symmetry plane. The turbulent flame velocity was modeled by the Shchelkin formula (Eq. (3)). The laminar flame velocity entering Eq. (3) was linearly interpolated using the data of look-up tables. Turbulence was modeled by the standard *k*–ε model. The computational grid was uniform with square cells 2 x 2 mm. The flame front in a computational cell was normally represented by no less than 15 segments. As seen from Fig. 3, the predicted flame front trajectories agree satisfactory with the measurements despite the 2D representation of essentially 3D phenomena in the experiments. It is worth noting that the numerical simulation is capable of adequate predicting the effect of various pressure waves on flame motion which is obvious from simultaneous appearance of crests on the curves.

Figure 4 shows the schematic of a straight PDE channel 40 mm wide with regular obstacles 2x2 mm size installed with a pitch of 20 mm along the entire channel. The boundary conditions and ignition were modeled in the same way as described above. In the calculations, only the upper part of the channel was considered with symmetry boundary conditions along the symmetry plane. For tracing possible autoignition events the preflame zone was represented by notional particles. The number of particles in each computational cell was controlled to be no less than 3 and no more than 12 with the mean value of 6. The autoignition of a particle was assumed to occur when the rate of temperature increase in this particle exceeded 10^6 K/s. The two-way coupling procedure between the particles and the mean flow was used. The autoignition of at least one particle in a cell was treated as the autoignition of all mixture throughout the cell volume. The channel configuration and the conditional treatment of preflame autoignition were used just to check the capability of the new code to predict the DDT phenomenon.

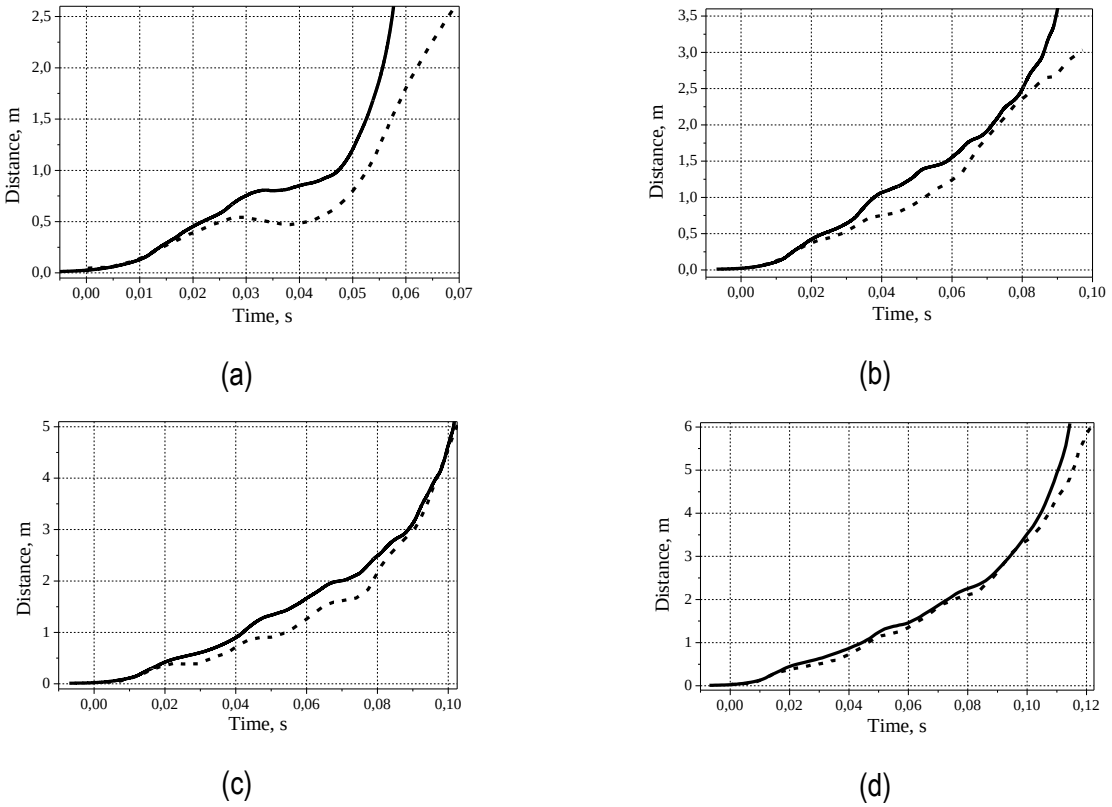

Figure 3: Comparison between predicted (solid curves) and measured [17] (dashed curves) distances traveled by the flame vs. time in 40x40 mm straight channels of different lengths filled with the stoichiometric propane–air mixture: (a) channel length 2.6 m, (b) 3.6 m, (c) 5.1 m, and (d) 6.1 m

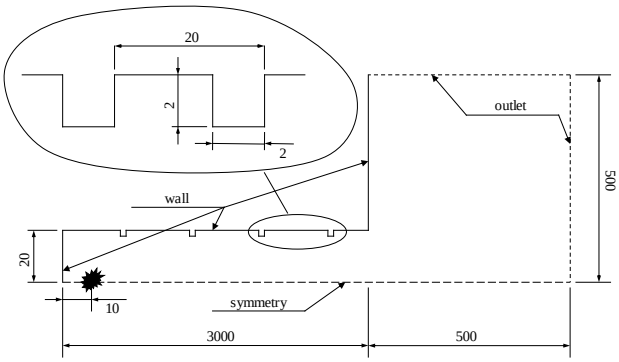

Figure 4: Schematic of a PDE channel. Dimensions are in millimeters.

Figure 5 shows the predicted temperature and propane mass fraction fields at different time (in ms) after ignition. The first six snapshots of temperature (left) and propane mass fraction (right) are plotted with a time interval of 5 ms. These snapshots correspond to the relatively slow initial stage of flame acceleration preceding preflame autoignition. The leading edges of wide red segments at the lines below the snapshots represent the instantaneous spatial positions of the flame front. The other six snapshots of temperature (lower snapshots) and propane mass fraction (upper snapshots) are plotted with a time interval of 0.05 ms. These snapshots correspond to the fast stage following the preflame autoignition ("explosion in the explosion" [5]). As is seen the Flame Tracking method avoids numerical diffusion of scalars through the flame front: the thin flame is always concentrated inside one computational cell separating unburned mixture from combustion products. In the course of flame propagation along the channel its overall shape exhibits various transformations, including a tulip-like shape (not shown in Fig. 5) in qualitative accordance with experimental observations. The

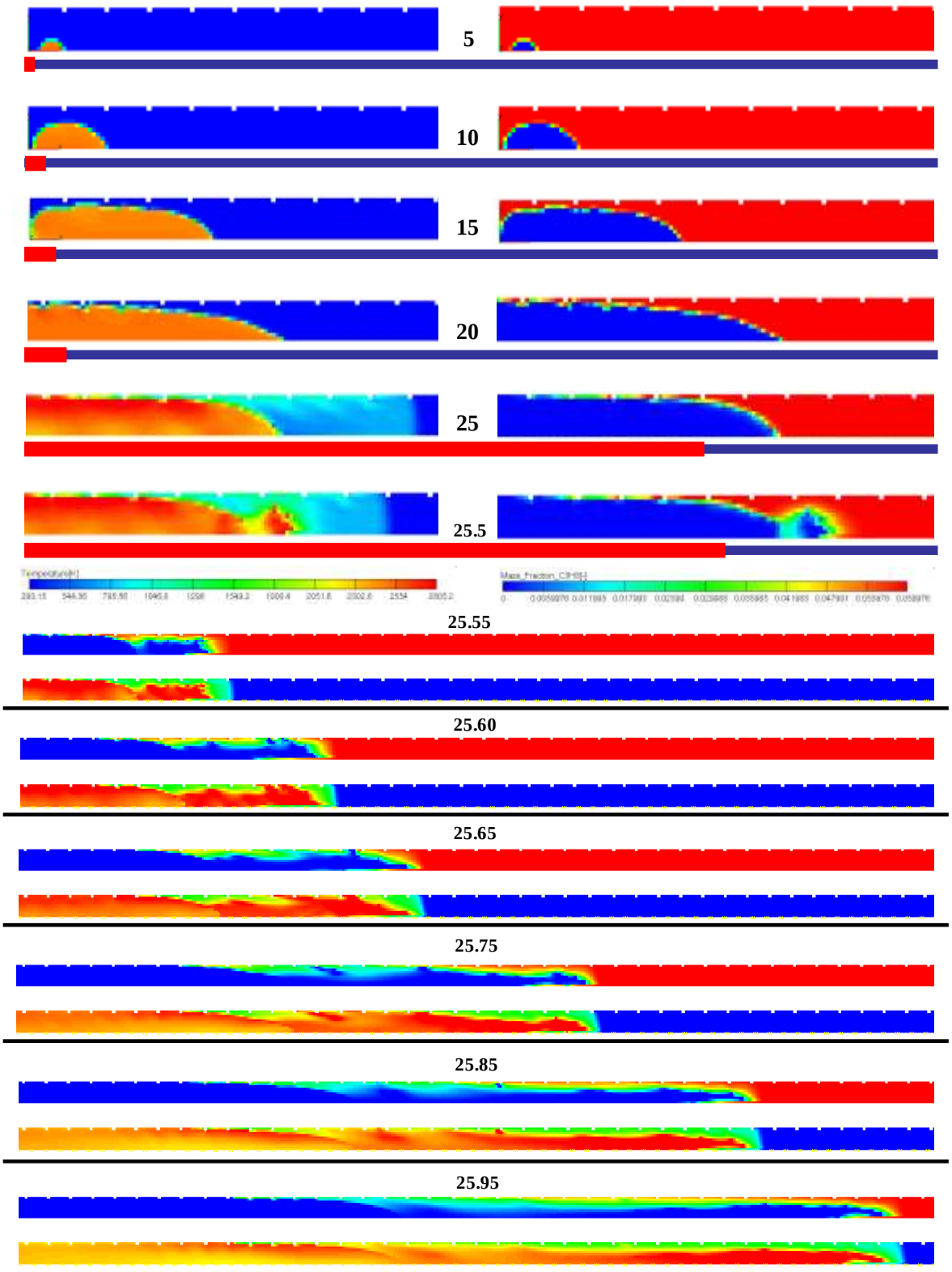

Figure 5: Predicted temperature and propane mass fraction fields at different time after ignition. Numbers correspond to time in ms

local instantaneous flame wrinkling increases with time. This is evident from the snapshots of propane mass fraction: with time the flame looks like smearing over more and more computational cells.

At the temperature snapshot corresponding to 25 ms one can clearly see the lead shock wave and bow shocks attached to the obstacles. The latter indicates that the postshock flow is supersonic. The instantaneous spatial temperature distributions in the preflame zone are nonuniform. At the snapshots corresponding to 25.5 ms preflame autoignition occurs. One can clearly see the exothermic centers (“hot spots”) in the preflame

zone. The hot spots are located in the central part of the channel rather than at its periphery due to the cold wall boundary condition. Interestingly, the cluster of exothermic centers originates at a certain distance from the flame front rather than directly ahead of it. This is caused by the existence of bow shocks and rarefaction fans generated by obstacles in the supersonic flow behind a lead shock wave. As can be seen from comparing the temperature snapshots at 25 and 25.5 ms, preflame autoignition occurs in the region compressed by the bow shock.

Contrary to the relatively slow initial stage of flame acceleration the evolution of the DDT process after preflame autoignition is very fast. This is demonstrated in Fig. 5 by the snapshots of temperature and propane mass fraction corresponding to 25.5 – 25.95 ms. In the presence of preflame autoignition two modes of combustion become possible simultaneously, namely the frontal and volumetric. Remind that the frontal mode is calculated using the Flame Tracking method whereas the volumetric mode is calculated using the Particle method. Formally, for adequate simulation of the DDT process one has to take into account the transition of the volumetric mode to the frontal one, in particular in the relatively cold near-wall region. At this stage of code development, this transition is not taken into account. Despite this fact does not affect much the DDT run-up distance and time (the volumetric mode spreads very fast predominantly in the longitudinal direction) it can affect the completeness of combustion and therefore the detonation velocity and other parameters (pressure, etc.). The snapshots corresponding to the fast stage of the DDT process indicate that a narrow near-wall region remains unburned whereas the central part of the channel burns in the shock-induced volumetric combustion mode resembling a detonation.

Figure 6 shows the predicted time histories of flame (solid curve) and shock wave (dashed curve) velocities in the run corresponding to Fig. 5. At time exceeding 20 ms, shock wave acceleration is seen to be considerably delayed with respect to flame acceleration. However at approximately 25 ms their propagation velocities begin quickly approach each other and abruptly change to 1650 m/s at 25.5 ms. This velocity is about 150 m/s lower than the CJ detonation velocity for the stoichiometric propane – air mixture (1804 m/s). The arising velocity deficit can be explained by incomplete combustion as well as by heat and momentum loss in the obstructed channel [19]. During the following 0.4 ms the shock wave – flame complex starts to decay. There can be several reasons for the decay but its study is beyond the scope of this paper.

Figure 7 shows the predicted spatial pressure distributions in the channel at different time after ignition. Pressure oscillations are caused by bow shocks and rarefaction waves generated by regular obstacles. The localized “explosion in the explosion” occurring at about 25.5 ms results in pressure rise up to 4 MPa.

Finally, Fig. 8 shows the predicted absolute pressure history at the head end of the channel (PDE thrust wall). The pressure curve is terminated when the head-end pressure drops to 0.16 MPa. The thrust is defined as

$$P(t) = \int_F [\,p(t) - p_0\,]dF$$

where F = 0.04 m^2/m is the specific surface area of the flat thrust wall. The thrust density is defined as:

$$P = \frac{1}{F}\int_0^{t_c} P(t)dt$$

where t_c is the combustion process time. For the case of Fig. 8, $t_c \approx 26$ ms and $P \approx 4804$ Pa-s. The fuel-based specific impulse is defined as

$$I_{sp,f} = F\frac{P}{m_f g}$$

where m_f is the specific fuel mass ($m_f \approx 0.0086$ kg/m at full fill conditions) and $g =$ 9.8 m/c^2 is the acceleration of gravity. Therefore the predicted specific impulse is equal to

$$I_{sp,f} = F\frac{P}{m_f g} \approx 0.04\frac{4804}{0.0086 \cdot 9.8} = 2280 \text{ s}$$

This number corresponds well with the specific impulse estimated for the propane fueled PDE based on the assumption of direct detonation initiation [20]. Note that the realistic PDE operation process additionally requires the finite time for filling the channel with the reactive mixture before ignition and purging the channel

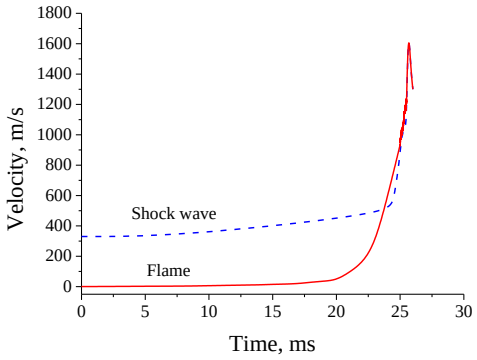

Figure 6: Time histories of flame (solid curve) and shock wave (dashed curve) velocities in the run corresponding to Fig. 5

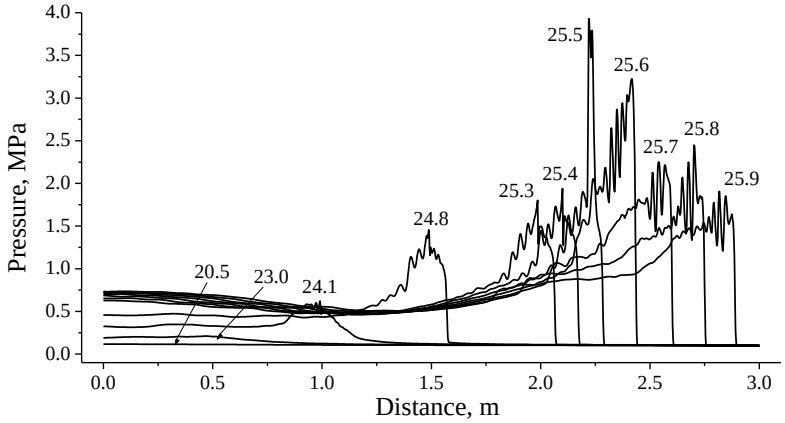

Figure 7: Predicted spatial pressure distributions in the channel at different time (in ms) after ignition.

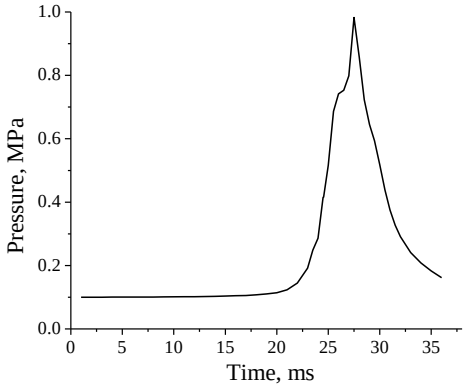

Figure 8: Predicted pressure history at the channel head end (PDE thrust wall).

with air after combustion products exhaust into the atmosphere. Therefore the cycle-averaged $I_{sp,f}$ will be somewhat different from the predicted value.

CONCLUDING REMARKS

A coupled FTP method combined with the look-up tables of laminar flame velocities and fuel oxidation has been developed and implemented into the CFD code. The method is parameter free and very efficient in terms of CPU requirements. It avoids numerical diffusion of scalar values through the flame front and provides spatial and temporal resolution of preflame autoignition sites. The algorithms have been tested for several 2D configurations with flame acceleration in smooth-walled channels of different length and with DDT in a channel

with regular obstacles and demonstrated good solution convergence and stability. The numerical simulation of DDT in the stoichiometric propane – air mixture made it possible to estimate the fuel-based specific impulse on the level of 2280 s which is close to the theoretical value obtained for direct detonation initiation. Further efforts will be directed on the improvement of the algorithm in terms of the transition from volumetric to frontal combustion in the near-wall regions.

ACKNOWLEDGMENTS

The authors thank Prof. Basevich V. Ya., and Dr. Belyaev A. A. for developing look-up tables. This work was supported by Russian Foundation for Basic Research (grant 08-08-00068).

REFERENCES

1. Lee J.H.S. The Detonation Phenomenon. Cambridge Univ. Press, 2008.
2. Bone W. A. and Fraser R. P., Philos. Trans. R. Soc. London, Ser. A, 1929, Vol. 228, p. 197.
3. Zel'dovich Ya. B. Theory of Combustion and Detonation of Gases, Akad. Nauk SSSR Publ., Moscow, 1944.
4. Shchelkin K. I. Fast Combustion and Spin Detonation of Gases, Voenizdat Publ., Moscow, 1949.
5. Oppenheim A. K. Introduction to Gasdynamics of Explosions, Springer, Wien, 1972.
6. Lee J.H.S., and Moen I., Prog. Energy Comb. Sci., 1980, Vol. 6, p. 359.
7. Higgins A.J., Pinard P., Yoshinaka A.K., Lee J.H.S. In: Pulse Detonation Engines, S.M. Frolov, ed., Torus Press, Moscow, 2006, p. 65.
8. Peraldi O., Knystautas R., and Lee J.H.S. Proc. Combust. Inst., 1986, Vol. 21, p. 1629.
9. Oran E., Gamezo V. Combustion and Flame, 2007, Vol. 148, p. 4.
10. Gamezo V., Ogawa T., Oran E. Combustion and Flame, 2008, Vol. 155, No. 1/2, p. 302.
11. Spalding D.B. Comb. Sci. Techn., 1976, Vol. 13, p. 3.
12. Pope S.B., Proc. Comb. Inst., 1990, Vol. 23, p. 591.
13. Peters N. Proc. Comb. Inst., 1986, Vol. 21, p. 1231.
14. Schelkin K.I., and Troshin, Ya.K. Gasdynamics of Combustion, USSR Acad. Sci. Publ., Moscow, 1963.
15. Frolov, S.M., Basevich, V.Ya., Neuhaus, M.G., andTatschl R. In: Advanced Computation and Analysis of Combustion, G.D. Roy, S.M. Frolov, and P. Givi, ed., ENAS Publ., Moscow, 1997, p. 537.
16. Frolov S.M., Ivanov V.S., Smetanyuk V.A., and Basara B. In: Proc. XXII YUMV International Automotive Conference with Exhibition "Science and Motor Vehicles," 14-16 April 2009, Belgrade, p. 9.
17. Kerampran S., Desbordes D., and Veyssiere B. In: Confined Detonations and Pulse Detonation Engines, G. Roy, S. Frolov, W. Santoro, and S. Tsyganov, ed., Torus Press, Moscow, 2003, p. 3.
18. Frolov S.M., Basevich V.Ya., Belyaev A.A., Posvyanskii V.S., and Radvogin Yu.B. Advances in Chemical Propulsion: Science to Technology, G.D. Roy, ed., CRC Press, Washington, D.C., 2001, Vol. 12, p. 191.
19. Zel'dovich Ya.B. and Kompaneets A.S. The Theory of Detonation, Gostekhteorizdat, Moscow, 1955.
20. Tangirala V.E., Dean A.J., and Harris P.G. ISABE Paper 2005-1048.